

Error Analysis of the Galerkin Finite Element Method for the Gray-Scott Model

Osama T. Al-Bairaqdar, Younis A. Sabawi*

Department of Mathematics, Faculty of Science and Health, Koya University, Koya 44023, Kurdistan Region, Iraq

Received August 19, 2025; Revised January 09, 2026; Accepted January 20, 2026

Cite This Paper in the Following Citation Styles

(a): [1] Osama T. Al-Bairaqdar, Younis A. Sabawi, "Error Analysis of the Galerkin Finite Element Method for the Gray-Scott Model," *Mathematics and Statistics*, Vol.14, No.1, pp. 55-67, 2026. DOI: 10.13189/ms.2026.140105.

(b): Osama T. Al-Bairaqdar, Younis A. Sabawi (2026). *Error Analysis of the Galerkin Finite Element Method for the Gray-Scott Model*. *Mathematics and Statistics*, 14(1), 55-67. DOI: 10.13189/ms.2026.140105.

Copyright ©2026 by authors, all rights reserved. Authors agree that this article remains permanently open access under the terms of the Creative Commons Attribution License 4.0 International License

Abstract This paper proposes an extensive finite element analysis of the one-dimensional Gray-Scott reaction-diffusion model (GSRDM), which is a fundamental framework for examining pattern formation in chemical and biological phenomena. A fully discrete numerical strategy was constructed utilizing the Galerkin finite element method (GFEM) for spatial discretization and the backward Euler (BE) scheme for temporal discretization. The nonlinear term is meticulously treated using a fully discrete formulation, preserving its authentic characteristics. The stability and convergence analysis of the discrete formulation is rigorously investigated by employing the error splitting and elliptic projection techniques with a special treatment for the nonlinear reaction terms. Numerical investigations employing a MATLAB script validated the predicted convergence rates and affirmed the precision of the proposed techniques. The impact of space and time-step refinements is examined comprehensively, supported by exact solutions and norm-based error analysis. A comparison with referenced works is discussed to demonstrate the effectiveness of the proposed scheme. This research offers a robust and adaptable framework for further studies on nonlinear reaction-diffusion systems.

Keywords Gray-Scott Model, Galerkin Finite Element Method, Stability and Convergence Analysis, Fully-discretization, Backward Euler Technique, Nonlinear Parabolic Problems

1 Introduction

Many significant events in the social, biological, and physical sciences can be quantitatively modeled using partial differential equations (PDEs) and systems of PDEs. They explain how unknown functions and their partial derivatives relate to independent variables. PDEs control a variety of intricate processes, including nonlinear motion, response, diffusion, equilibrium, and numerous other difficult phenomena and mathematical issues, even if the underlying differential relationships may seem straightforward [1–3]. One of the most well-known reaction-diffusion models is the Gray-Scott model (GSM), which was developed based on the chemical reaction model by Peter Gray and Steve Scott [4]. This model involves equations that describe the evolution of the concentrations of chemical species over time, incorporating reaction terms and diffusion operators to accurately capture the system's dynamics.

Consider a bounded domain $\mathcal{D} := [-L, L] \subset \mathbb{R}$, with a boundary $\partial\mathcal{D} = \{-L, L\}$. Then, the general form of the GSM is:

$$\partial_t z - \delta_z z_{xx} = C_z(z, w), \quad (x, t) \in \mathcal{D} \times (0, T], \quad (1)$$

$$\partial_t w - \delta_w w_{xx} = C_w(z, w), \quad (x, t) \in \mathcal{D} \times (0, T]. \quad (2)$$

where

$$\partial_t z = \frac{\partial z}{\partial t}, \quad \partial_t w = \frac{\partial w}{\partial t},$$

$z = z(x, t) : (-L, L) \times (0, T] \mapsto \mathbb{R}$ and $w = w(x, t) : (-L, L) \times (0, T] \mapsto \mathbb{R}$ represent the concentrations of the two chemical species. δ_z and δ_w are the diffusion rates of the species z and w , respectively, such that $0 < C_1 < \delta_z, \delta_w < C_2$

for some positive $C_j (j = 1, 2)$,

$$\begin{aligned} C_z &:= \alpha(1 - z) - zw^2, \\ C_w &:= zw^2 - \beta w, \end{aligned}$$

$\alpha, \beta \in \mathbb{R}$ are the reaction rates that determine how the concentrations of the species change due to chemical reactions. The term zw^2 represents the reaction in which species z is converted to species w , and $(1 - z)$ and βw represent the generation and depletion of z and w , respectively.

Numerous scholars have examined reaction-diffusion models both numerically and analytically [5–10]. Rodrigo and Mimura [11] presented a general technique to identify exact travelling with standing wave approaches of reaction-diffusion models as well as nonlinear wave equations. In addition, various researchers have achieved numerical solutions for GSM with the implementation of diverse techniques. Hale [12] achieved distinct nontrivial stationary patterns in a one-dimensional GSRD system for cubic autocatalysis. Rasheed and Manaa [13] used finite difference methods in conjunction with a successive approximation strategy. Owolabi et al. [14] implemented a combination of higher-order systems. Korkmaz et al. [15] used differential quadrature alongside the implicit Rosenbrock approach of third-fourth order and exponential B-splines. Mittal and Rohila [16] numerically solved the GSM using a modified cubic B-spline. Jiwari et al. [17] identified the GSM patterns by implementing the differential quadrature technique. An algorithm for GSM model was introduced by Onarcu [18]. Jiwari and Yadav [19] solved the proposed model by Galerkin finite element techniques.

Recently, a two-dimensional nonlinear coupled GS system was simulated by Amin and Mashat [20] using a finite difference approach mixed with a finite volume method. Giampaolo et al [21] presented a computational analysis utilizing PINN to address a system of nonlinear PDEs that was employed to solve the GSM, a reaction-diffusion system characterized by an irreversible reaction between two reactants. Onarcu et al. [22] numerically analysed the GSM employing a quintic trigonometric B-spline. Ali and Saleem [23] employed an innovative high-order numerical technique utilizing the Chebyshev spectral method to investigate the non homogeneous steady-state solutions of the GSM. Al-Jeaid [24] introduced a new approach to solve a system of a coupled diffusion kinetic problem with one delayed neutron precursor concentration in Cartesian geometry. It transforms the given PDEs into linear ordinary differential equations (ODEs) and obtains the solution through a simple analytical procedure. This method avoids natural transformations like Laplace transform and provides a direct solution, reducing computational work. Cappanera et al. [25] presented a research that expands a model to incorporate non-local chemical dispersion, concentrating on strictly positive, symmetric L1 convolution kernels with a limited second moment. It demonstrates minor weak solutions under non-local boundary conditions and formulates a finite element numerical method. This model can also be solved using the Haar wavelet method, as demonstrated in earlier studies [26–28].

The present study is devoted to the mathematical and numerical investigation of a one-dimensional GSRD system. A

detailed weak form is derived, and a semi-discretization using Galerkin finite element method (GFEM) in space is presented. The fully discrete scheme is constructed using the backward Euler technique for temporal discretization, detailed convergence and stability analyses are investigated, and both error splitting and elliptic projection techniques are employed to derive optimal order *a priori* error estimates in the $\mathcal{L}^\infty(\mathcal{L}^2)$ -norms.

The novelty of this work lies in the following contributions:

- A comprehensive derivation of both semi-discrete and fully discrete formulations was supplemented by stability and consistency analyses.
- A rigorous convergence analysis of the fully discrete GSM was performed using error splitting and elliptic projection techniques.
- The nonlinear term is meticulously treated by full discretization, preserving its authentic characteristics with an emphasis on robustness and convergence efficiency.
- Detailed numerical simulations that verify the theoretical results, including spatial and temporal convergence studies, are performed using an exact solution.

The rest of this study is organized as follows: Section 2 presents the basic concepts, weak formulation and the finite element spatial discretization. Section 3 details the full discretization utilizing the BE scheme with the stability and convergence analysis of the proposed methodology. Section 4 is devoted to the computational framework and calculations of the main matrices with special treatment for the nonlinear term. Section 5 provides numerical experiments to validate the theoretical findings. Finally, Section 6 discusses the conclusions drawn and future studies.

2 Preliminaries

This section introduces the fundamental concepts and definitions that are useful for deriving our main results.

2.1 Basic Notation and Function Setting for GSM

Suppose a domain $\mathcal{D} = [-L, L] \subset \mathbb{R}$. we define the spaces $\mathcal{L}^2(\mathcal{D})$ and $\mathcal{L}^\infty(\mathcal{D})$ of the Lebesgue integrable functions on \mathcal{D} as [29]:

$$\begin{aligned} \mathcal{L}^2(\mathcal{D}) &:= \left\{ \phi : \mathcal{D} \rightarrow \mathbb{R} \mid \int_{\mathcal{D}} |\phi(x)|^2 dx < \infty \right\}, \\ \mathcal{L}^\infty(\mathcal{D}) &:= \left\{ \phi : \mathcal{D} \rightarrow \mathbb{R} \mid \text{ess} \cdot \sup_{x \in \mathcal{D}} |\phi(x)| < \infty \right\}, \end{aligned}$$

equipped with the norms

$$\begin{aligned} \|\phi\|_{\mathcal{L}^2(\mathcal{D})} &:= \left(\int_{\mathcal{D}} |\phi(x)|^2 dx \right)^{1/2}, \\ \|\phi\|_{\mathcal{L}^\infty(\mathcal{D})} &:= \text{ess} \cdot \sup_{x \in \mathcal{D}} \|\phi(x)\| \end{aligned}$$

we also define $\mathcal{H}^1(\mathcal{D}) \equiv W^{1,2}(\mathcal{D})$ and $\mathcal{H}^2(\mathcal{D}) \equiv W^{2,2}(\mathcal{D})$ the Sobolev spaces,

$$\mathcal{H}^1(\mathcal{D}) = \left\{ \phi \in \mathcal{L}^2(\mathcal{D}) \mid \frac{\partial \phi}{\partial x_i} \in \mathcal{L}^2(\mathcal{D}), i = 0, 1, \dots, n \right\},$$

with the norm

$$\|\phi\|_{\mathcal{H}^1(\mathcal{D})} := \left(\|\phi\|_{\mathcal{L}^2(\mathcal{D})}^2 + \sum_{i=1}^n \left\| \frac{\partial \phi}{\partial x_i} \right\|_{\mathcal{L}^2(\mathcal{D})}^2 \right)^{1/2},$$

and semi-norm

$$|\phi|_{\mathcal{H}^1(\mathcal{D})} := \left(\sum_{i=1}^n \left\| \frac{\partial \phi}{\partial x_i} \right\|_{\mathcal{L}^2(\mathcal{D})}^2 \right)^{1/2},$$

and for all $i, j = 0, 1, \dots, n$,

$$\mathcal{H}^2(\mathcal{D}) = \left\{ \phi \in \mathcal{L}^2(\mathcal{D}) \mid \frac{\partial \phi}{\partial x_i}, \frac{\partial^2 \phi}{\partial x_i \partial x_j} \in \mathcal{L}^2(\mathcal{D}) \right\},$$

with the norm

$$\|\phi\|_{\mathcal{H}^2(\mathcal{D})} := \left(\|\phi\|_{\mathcal{L}^2(\mathcal{D})}^2 + \sum_{i=1}^n \left\| \frac{\partial \phi}{\partial x_i} \right\|_{\mathcal{L}^2(\mathcal{D})}^2 + \sum_{i=1}^n \left\| \frac{\partial^2 \phi}{\partial x_i \partial x_j} \right\|_{\mathcal{L}^2(\mathcal{D})}^2 \right)^{1/2}$$

and semi-norm

$$|\phi|_{\mathcal{H}^2(\mathcal{D})} := \left(\sum_{i=1}^n \left\| \frac{\partial^2 \phi}{\partial x_i \partial x_j} \right\|_{\mathcal{L}^2(\mathcal{D})}^2 \right)^{1/2}.$$

We also define a special space denoted by $\mathcal{H}_0^1(\mathcal{D})$, which for a sufficiently smooth $\partial\mathcal{D}$, can be identified as

$$\mathcal{H}_0^1(\mathcal{D}) := \{ \phi \in \mathcal{H}^1(\mathcal{D}) \mid \phi = 0 \text{ on } \partial\mathcal{D} \}.$$

For notational convenience, we shall denote the spaces $\mathcal{L}^2(\mathcal{D})$, $\mathcal{H}^1(\mathcal{D})$, and $\mathcal{H}^2(\mathcal{D})$ by \mathcal{L}^2 , \mathcal{H}^1 , and \mathcal{H}^2 , respectively, unless otherwise specified.

2.2 Weak Formulation

With the notations above, the weak form of GSM can be obtained by multiplying (1) and (2) by test functions $v, \tilde{v} \in \mathcal{H}^1(\mathcal{D})$, integrating by part over domain \mathcal{D} and substituting the homogeneous Neumann boundary conditions; thus, the weak form reads: For all $t \in (0, T]$, find $z, w \in \mathcal{H}^1(\mathcal{D})$, such that, for all $v, \tilde{v} \in \mathcal{H}^1(\mathcal{D})$

$$\langle \partial_t z, v \rangle + \mathfrak{B}(z, v) = \langle \mathcal{C}_z(z, w), v \rangle, \tag{3}$$

$$\langle \partial_t w, \tilde{v} \rangle + \mathfrak{B}(w, \tilde{v}) = \langle \mathcal{C}_w(z, w), \tilde{v} \rangle, \tag{4}$$

the inner product $\langle \cdot, \cdot \rangle$ is defined by

$$\langle \phi, \psi \rangle = \int_{\mathcal{D}} \phi \cdot \psi dx$$

and the continuous bilinear form $\mathfrak{B}(\cdot, \cdot)$ on $\mathcal{H}_0^1(\mathcal{D}) \times \mathcal{H}_0^1(\mathcal{D})$ is defined by

$$\mathfrak{B}(\phi, v) := \delta_\phi \int_{\mathcal{D}} \frac{\partial \phi}{\partial x} \cdot \frac{\partial v}{\partial x} dx = \delta_\phi \langle \nabla \phi, \nabla v \rangle.$$

2.3 Finite element approximation

To approximate our model (3),(4), we exchange the space \mathcal{H}^1 by a finite dimensional subspace $\mathcal{V}^h \subset \mathcal{H}^1(\mathcal{D})$, which consists of continuous piecewise Lagrange linear polynomials $\{\varphi_j\}_{j=1}^N$, called "hat" function associated with the uniform discretization $(x_j, x_{j+1}), j = 1, \dots, N - 1$ of the space domain \mathcal{D} , with $x_j - x_{j-1} = h$.

Thus, the spatial semi-discrete finite element formulation for GSM (1),(2) reads: Find $z_h, w_h \in \mathcal{V}^h$, for all $t \in (0, T]$, such that

$$\langle \partial_t z_h, v_h \rangle + \mathfrak{B}(z_h, v_h) = \langle \mathcal{C}_z(z_h, w_h), v_h \rangle, \quad v_h \in \mathcal{H}^1(\mathcal{D}), \tag{5}$$

$$\langle \partial_t w_h, \tilde{v}_h \rangle + \mathfrak{B}(w_h, \tilde{v}_h) = \langle \mathcal{C}_w(z_h, w_h), \tilde{v}_h \rangle, \quad \tilde{v}_h \in \mathcal{H}^1(\mathcal{D}). \tag{6}$$

Because the space \mathcal{V}^h is spanned by the basis function $\{\varphi_j\}_{j=1}^N$, we suppose that any approximations z_h, w_h of z, w , respectively, can be expressed as a linear combination of the aforementioned basis functions, that is,

$$z_h(x, t) = \sum_{j=1}^N Z_j(t) \varphi_j(x), \tag{7}$$

$$w_h(x, t) = \sum_{j=1}^N W_j(t) \varphi_j(x), \tag{8}$$

where, $Z = [Z_1, Z_2, \dots, Z_N]$ and $W = [W_1, W_2, \dots, W_N]$ represent the unknowns vectors, and $\varphi_j \in \mathcal{V}^h, j = 0, 1, \dots, N$.

3 Fully Discretization

This section emphasizes the temporal fully-discrete formulation utilizing the BE technique. Consequently, the time interval $(0, T]$ is discretized into a finite number of sub-intervals $(t^{m-1}, t^m], m = 1, 2, \dots, N_t$, provided $t^0 = 0$ and $t^{N_t} = T$, we define the local time step as $\tau = t^m - t^{m-1}$, such that $\tau = \frac{T}{N_t}$. Let

$$\partial_t z_h = \frac{z_h^m - z_h^{m-1}}{\tau}, \quad \partial_t w_h = \frac{w_h^m - w_h^{m-1}}{\tau},$$

substitute in (5) and (6), thus, the fully-discrete BE approximation of the GSM is expressed as, for all $v, \tilde{v} \in \mathcal{V}^h$

$$\left\langle \frac{z_h^m - z_h^{m-1}}{\tau}, v_h \right\rangle + \mathfrak{B}(z_h^m, v_h) = \langle \mathcal{C}_z(z_h^m, w_h^m), v_h \rangle, \tag{9}$$

$$\left\langle \frac{w_h^m - w_h^{m-1}}{\tau}, \tilde{v}_h \right\rangle + \mathfrak{B}(w_h^m, \tilde{v}_h) = \langle \mathcal{C}_w(z_h^m, w_h^m), \tilde{v}_h \rangle. \tag{10}$$

with

$$z_h(x, 0) = z_{0,h}, \quad w_h(x, 0) = w_{0,h},$$

where $z_{0,h}, w_{0,h} \in \mathcal{V}^h$ are appropriate approximations to z_0, w_0 respectively.

3.1 Stability Analysis Theorem for the Fully-Discrete GSM

Consider the semi-discrete GSM, where $z_h(t), w_h(t)$ are finite element approximations in a spatially discretized space $\mathcal{V}^h \subset \mathcal{H}^1(\mathcal{D})$. Thus, we present the following stability theorem:

Theorem 3.1. *Let $\mathcal{V}^h \subset \mathcal{H}^1(\mathcal{D})$. By choosing $\tau < \frac{1}{2C(1+M^2)}$, for sufficiently small C and M , then, the fully-discrete scheme is stable.*

Proof. The backward Euler scheme can be directly utilized on (3) and (4) to obtain:

$$\begin{aligned} \left\langle \frac{z^m - z^{m-1}}{\tau}, v \right\rangle + \mathfrak{B}(z^m, v) &= \langle \mathcal{C}_z(z, w), v \rangle, \\ \left\langle \frac{w^m - w^{m-1}}{\tau}, \check{v} \right\rangle + \mathfrak{B}(w^m, \check{v}) &= \langle \mathcal{C}_w(z, w), \check{v} \rangle. \end{aligned}$$

Simplifying

$$\langle z^m, v \rangle + \tau \delta_z \langle z_x^m, v_x \rangle = \langle z^{m-1}, v \rangle + \tau \langle \mathcal{C}_z(z^m, w^m), v \rangle. \quad (11)$$

$$\langle w^m, \check{v} \rangle + \tau \delta_w \langle w_x^m, \check{v}_x \rangle = \langle w^{m-1}, \check{v} \rangle + \tau \langle \mathcal{C}_w(z^m, w^m), \check{v} \rangle. \quad (12)$$

Same process can be applied to (5),(6) to obtain

$$\langle z_h^m, v_h \rangle + \tau \delta_z \langle z_{h,x}^m, v_{h,x} \rangle = \langle z_h^{m-1}, v_h \rangle + \tau \langle \mathcal{C}_z(z_h^m, w_h^m), v_h \rangle, \quad (13)$$

$$\langle w_h^m, \check{v}_h \rangle + \tau \delta_w \langle w_{h,x}^m, \check{v}_{h,x} \rangle = \langle w_h^{m-1}, \check{v}_h \rangle + \tau \langle \mathcal{C}_w(z_h^m, w_h^m), \check{v}_h \rangle. \quad (14)$$

Subtracting (13) from (11) and (14) from (12) to get

$$\begin{aligned} \langle \varepsilon^m, v_h \rangle + \tau \delta_z \langle \varepsilon_x^m, v_{h,x} \rangle &= \langle \varepsilon^{m-1}, v_h \rangle \\ &+ \tau \langle \mathcal{C}_z(z^m, w^m) - \mathcal{C}_z(z_h^m, w_h^m), v_h \rangle, \\ \langle \check{\varepsilon}^m, \check{v}_h \rangle + \tau \delta_w \langle \check{\varepsilon}_x^m, \check{v}_{h,x} \rangle &= \langle \check{\varepsilon}^{m-1}, \check{v}_h \rangle \\ &+ \tau \langle \mathcal{C}_w(z^m, w^m) - \mathcal{C}_w(z_h^m, w_h^m), \check{v}_h \rangle. \end{aligned}$$

Where,

$$\varepsilon^m = z^m - z_h^m, \quad \check{\varepsilon}^m = w^m - w_h^m$$

Now, setting $v_h = \varepsilon^m$, $\check{v}_h = \check{\varepsilon}^m$ we obtain

$$\begin{aligned} \langle \varepsilon^m, \varepsilon^m \rangle + \tau \delta_z \langle \varepsilon_x^m, \varepsilon_x^m \rangle &= \langle \varepsilon^{m-1}, \varepsilon^m \rangle \\ &+ \tau \langle \mathcal{C}_z(z^m, w^m) - \mathcal{C}_z(z_h^m, w_h^m), \varepsilon^m \rangle, \\ \langle \check{\varepsilon}^m, \check{\varepsilon}^m \rangle + \tau \delta_w \langle \check{\varepsilon}_x^m, \check{\varepsilon}_x^m \rangle &= \langle \check{\varepsilon}^{m-1}, \check{\varepsilon}^m \rangle \\ &+ \tau \langle \mathcal{C}_w(z^m, w^m) - \mathcal{C}_w(z_h^m, w_h^m), \check{\varepsilon}^m \rangle. \end{aligned}$$

Thus,

$$\begin{aligned} \|\varepsilon^m\|_{\mathcal{L}^2}^2 + \tau \delta_z \|\varepsilon_x^m\|_{\mathcal{L}^2}^2 &= \langle \varepsilon^{m-1}, \varepsilon^m \rangle \\ &+ \tau \langle \mathcal{C}_z(z^m, w^m) - \mathcal{C}_z(z_h^m, w_h^m), \varepsilon^m \rangle, \end{aligned} \quad (15)$$

$$\begin{aligned} \|\check{\varepsilon}^m\|_{\mathcal{L}^2}^2 + \tau \delta_w \|\check{\varepsilon}_x^m\|_{\mathcal{L}^2}^2 &= \langle \check{\varepsilon}^{m-1}, \check{\varepsilon}^m \rangle \\ &+ \tau \langle \mathcal{C}_w(z^m, w^m) - \mathcal{C}_w(z_h^m, w_h^m), \check{\varepsilon}^m \rangle. \end{aligned} \quad (16)$$

To bound the nonlinear inner products on the right hand side of (15), we have:

$$\begin{aligned} &\langle \mathcal{C}_z(z^m, w^m) - \mathcal{C}_z(z_h^m, w_h^m), \varepsilon^m \rangle \\ &\leq |\langle \mathcal{C}_z(z^m, w^m) - \mathcal{C}_z(z_h^m, w_h^m), \varepsilon^m \rangle| \\ &= |\langle -\alpha(z^m - z_h^m) - (z^m(w^m)^2 - z_h^m(w_h^m)^2), \varepsilon^m \rangle| \\ &= |\langle -\alpha\varepsilon^m - (z^m(w^m)^2 - z_h^m(w_h^m)^2), \varepsilon^m \rangle|. \end{aligned} \quad (17)$$

Applying the triangular inequality

$$\begin{aligned} &\langle \mathcal{C}_z(z^m, w^m) - \mathcal{C}_z(z_h^m, w_h^m), \varepsilon^m \rangle \\ &\leq \alpha \|\varepsilon^m\|_{\mathcal{L}^2}^2 + |\langle (z^m(w^m)^2 - z_h^m(w_h^m)^2), \varepsilon^m \rangle| \\ &= \alpha \|\varepsilon^m\|_{\mathcal{L}^2}^2 \\ &\quad + |\langle z^m((w^m)^2 - (w_h^m)^2) + (z^m - z_h^m)(w_h^m)^2, \varepsilon^m \rangle| \\ &= \alpha \|\varepsilon^m\|_{\mathcal{L}^2}^2 \\ &\quad + |\langle z^m(w^m - w_h^m)(w^m + w_h^m) + \varepsilon^m(w_h^m)^2, \varepsilon^m \rangle| \\ &\leq \alpha \|\varepsilon^m\|_{\mathcal{L}^2}^2 \\ &\quad + |\langle z^m(\check{\varepsilon}^m)(w^m + w_h^m), \varepsilon^m \rangle| + |\langle \varepsilon^m(w_h^m)^2, \varepsilon^m \rangle|. \end{aligned}$$

Assume that z^m, w^m, w_h^m are bounded in $\mathcal{L}^\infty(\mathcal{D})$ by a constant $M > 0$. Then:

$$\begin{aligned} \langle \mathcal{C}_z(z^m, w^m) - \mathcal{C}_z(z_h^m, w_h^m), \varepsilon^m \rangle &\leq \alpha \|\varepsilon^m\|_{\mathcal{L}^2}^2 \\ &+ \|z^m\|_{\mathcal{L}^\infty} \|w^m + w_h^m\|_{\mathcal{L}^\infty} \|\check{\varepsilon}^m\|_{\mathcal{L}^2} \|\varepsilon^m\|_{\mathcal{L}^2} \\ &+ \|w_h^m\|_{\mathcal{L}^\infty}^2 \|\varepsilon^m\|_{\mathcal{L}^2}^2 \\ &\leq \alpha \|\varepsilon^m\|_{\mathcal{L}^2}^2 + CM^2 \|\check{\varepsilon}^m\|_{\mathcal{L}^2} \|\varepsilon^m\|_{\mathcal{L}^2} + M^2 \|\varepsilon^m\|_{\mathcal{L}^2}^2 \end{aligned}$$

Applying Young's Inequality

$$\begin{aligned} \langle \mathcal{C}_z(z^m, w^m) - \mathcal{C}_z(z_h^m, w_h^m), \varepsilon^m \rangle &\leq \alpha \|\varepsilon^m\|_{\mathcal{L}^2}^2 \\ &+ \frac{CM^2}{2} (\|\check{\varepsilon}^m\|_{\mathcal{L}^2}^2 + \|\varepsilon^m\|_{\mathcal{L}^2}^2) + M^2 \|\varepsilon^m\|_{\mathcal{L}^2}^2 \end{aligned}$$

Simplifying

$$\begin{aligned} \langle \mathcal{C}_z(z^m, w^m) - \mathcal{C}_z(z_h^m, w_h^m), \varepsilon^m \rangle \\ \leq C(1 + M^2) (\|\varepsilon^m\|_{\mathcal{L}^2}^2 + \|\check{\varepsilon}^m\|_{\mathcal{L}^2}^2). \end{aligned} \quad (18)$$

Similarly,

$$\begin{aligned} \langle \mathcal{C}_w(z^m, w^m) - \mathcal{C}_w(z_h^m, w_h^m), \check{\varepsilon}^m \rangle \\ \leq C(1 + M^2) (\|\check{\varepsilon}^m\|_{\mathcal{L}^2}^2 + \|\varepsilon^m\|_{\mathcal{L}^2}^2). \end{aligned} \quad (19)$$

Substituting (18) and (19) into (15) and (16), respectively, yields

$$\begin{aligned} \|\varepsilon^m\|_{\mathcal{L}^2}^2 + \tau \delta_z \|\varepsilon_x^m\|_{\mathcal{L}^2}^2 &\leq \|\varepsilon^{m-1}\|_{\mathcal{L}^2} \|\varepsilon^m\|_{\mathcal{L}^2} \\ &+ \tau C(1 + M^2) (\|\varepsilon^m\|_{\mathcal{L}^2}^2 + \|\check{\varepsilon}^m\|_{\mathcal{L}^2}^2), \\ \|\check{\varepsilon}^m\|_{\mathcal{L}^2}^2 + \tau \delta_w \|\check{\varepsilon}_x^m\|_{\mathcal{L}^2}^2 &\leq \|\check{\varepsilon}^{m-1}\|_{\mathcal{L}^2} \|\check{\varepsilon}^m\|_{\mathcal{L}^2} \\ &+ \tau C(1 + M^2) (\|\varepsilon^m\|_{\mathcal{L}^2}^2 + \|\check{\varepsilon}^m\|_{\mathcal{L}^2}^2). \end{aligned}$$

Applying Young's inequality

$$\begin{aligned} \|\varepsilon^m\|_{\mathcal{L}^2}^2 + \tau \delta_z \|\varepsilon_x^m\|_{\mathcal{L}^2}^2 &\leq \frac{1}{2} (\|\varepsilon^{m-1}\|_{\mathcal{L}^2}^2 + \|\varepsilon^m\|_{\mathcal{L}^2}^2) \\ &+ \tau C(1 + M^2) (\|\varepsilon^m\|_{\mathcal{L}^2}^2 + \|\check{\varepsilon}^m\|_{\mathcal{L}^2}^2), \end{aligned}$$

$$\begin{aligned} \|\varepsilon^m\|_{\mathcal{L}^2}^2 + \tau\delta_w \|\tilde{\varepsilon}_x^m\|_{\mathcal{L}^2}^2 &\leq \frac{1}{2} \left(\|\tilde{\varepsilon}^{m-1}\|_{\mathcal{L}^2}^2 + \|\varepsilon^m\|_{\mathcal{L}^2}^2 \right) \\ &\quad + \tau C (1 + M^2) \left(\|\varepsilon^m\|_{\mathcal{L}^2}^2 + \|\tilde{\varepsilon}^m\|_{\mathcal{L}^2}^2 \right). \end{aligned}$$

Simplifying, we obtain

$$\begin{aligned} \left(\frac{1}{2} - \tau C (1 + M^2) \right) \|\varepsilon^m\|_{\mathcal{L}^2}^2 + \tau\delta_z \|\varepsilon_x^m\|_{\mathcal{L}^2}^2 \\ \leq \frac{1}{2} \|\varepsilon^{m-1}\|_{\mathcal{L}^2}^2 + \tau C (1 + M^2) \|\tilde{\varepsilon}^m\|_{\mathcal{L}^2}^2, \end{aligned} \tag{20}$$

$$\begin{aligned} \left(\frac{1}{2} - \tau C (1 + M^2) \right) \|\tilde{\varepsilon}^m\|_{\mathcal{L}^2}^2 + \tau\delta_w \|\tilde{\varepsilon}_x^m\|_{\mathcal{L}^2}^2 \\ \leq \frac{1}{2} \|\tilde{\varepsilon}^{m-1}\|_{\mathcal{L}^2}^2 + \tau C (1 + M^2) \|\varepsilon^m\|_{\mathcal{L}^2}^2. \end{aligned} \tag{21}$$

For (20), since $\tau\delta_z \|\varepsilon_x^m\|_{\mathcal{L}^2}^2 \geq 0$, thus

$$\begin{aligned} \left(\frac{1}{2} - \tau C (1 + M^2) \right) \|\varepsilon^m\|_{\mathcal{L}^2}^2 \\ \leq \frac{1}{2} \|\varepsilon^{m-1}\|_{\mathcal{L}^2}^2 + \tau C (1 + M^2) \|\tilde{\varepsilon}^m\|_{\mathcal{L}^2}^2. \end{aligned}$$

To maintain coercivity, we set $\tau < \frac{1}{2C(1+M^2)}$ in the above inequality, so that the coefficient $(\frac{1}{2} - \tau C(1 + M^2))$ is positive. Suppose that $\|\tilde{\varepsilon}^m\|_{\mathcal{L}^2}^2 \leq C\|\varepsilon^m\|_{\mathcal{L}^2}^2$, which holds when the errors in z and w are comparably bounded. Then:

$$\left(\frac{1}{2} - \tau C(1 + M^2)(1 + C) \right) \|\varepsilon^m\|_{\mathcal{L}^2}^2 \leq \frac{1}{2} \|\varepsilon^{m-1}\|_{\mathcal{L}^2}^2.$$

Let

$$\lambda := \frac{\frac{1}{2}}{\frac{1}{2} - \tau C(1 + M^2)(1 + C)} > 1.$$

Then by recursion:

$$\|\varepsilon^m\|_{\mathcal{L}^2}^2 \leq \lambda^m \|\varepsilon^0\|_{\mathcal{L}^2}^2.$$

Since τ is small, λ is close to 1; therefore, the error remains bounded.

$$\|\varepsilon^m\|_{\mathcal{L}^2}^2 \leq C\|\varepsilon^0\|_{\mathcal{L}^2}^2.$$

Similarly, for (21) we obtain

$$\|\tilde{\varepsilon}^m\|_{\mathcal{L}^2}^2 \leq C\|\tilde{\varepsilon}^0\|_{\mathcal{L}^2}^2.$$

This completes the proof. \square

3.2 Convergence Analysis for the Fully-Discrete GSM

This subsection discusses the convergence theorem for the BE fully-discrete scheme, to this end we introduce some important concepts.

Definition 3.1 (Elliptic Projection Operator). $\forall \phi \in \mathcal{H}_0^1(\mathcal{D})$, we define a projection operator \mathcal{P}_h onto \mathcal{V}^h by

$$\mathfrak{B}(\mathcal{P}_h \phi, \psi) = \mathfrak{B}(\phi, \psi), \quad \forall \psi \in \mathcal{V}^h.$$

Furthermore, for any $\phi \in \mathcal{H}^1(\mathcal{D}) \cap \mathcal{H}_0^1(\mathcal{D})$, the operator \mathcal{P}_h satisfies:

$$\|\mathcal{P}_h \phi - \phi\|_{\mathcal{L}^2} + h \|\nabla(\mathcal{P}_h \phi - \phi)\|_{\mathcal{L}^2} \leq Ch^2.$$

Thus, we can split the total errors for the GSM into two components using the elliptic projection \mathcal{P}_h as follows:

$$\begin{aligned} \hat{\varepsilon}^m &= z(t^m) - z^m := \hat{\eta}^m + \hat{\theta}^m, \\ \tilde{\varepsilon}^m &= w(t^m) - w^m := \tilde{\eta}^m + \tilde{\theta}^m, \end{aligned}$$

where

$$\begin{aligned} \hat{\eta}^m &= z(t^m) - \mathcal{P}_h z(t^m), & \hat{\theta}^m &= \mathcal{P}_h z(t^m) - z_h^m, \\ \tilde{\eta}^m &= w(t^m) - \mathcal{P}_h w(t^m), & \tilde{\theta}^m &= \mathcal{P}_h w(t^m) - w_h^m. \end{aligned}$$

Now, we present the following a priori convergence theorem:

Theorem 3.2. Assume z, w are exact solutions for the GSM (1) and (2), and suppose z_h^m, w_h^m are the fully discrete FE approximations using the backward Euler time discretization scheme (9) and (10). Then, there is a constant C , independent of h and τ , such that

$$\max_{1 \leq m \leq M} (\|z(t^m) - z_h^m\|_{\mathcal{L}^2} + \|w(t^m) - w_h^m\|_{\mathcal{L}^2}) \leq C(\tau + h^2).$$

Proof. By subtracting the fully discrete equations (9) and (10) from the elliptic projection of the weak form and applying error splitting, we obtain the error equations:

$$\begin{aligned} \left\langle \frac{\hat{\theta}^m - \hat{\theta}^{m-1}}{\tau}, v_h \right\rangle + \delta_z \langle \hat{\theta}_x^m, v_{x,h} \rangle \\ = \langle \mathcal{C}_z(z^m, w^m) - \mathcal{C}_z(z_h^m, w_h^m), v_h \rangle + R^m(v_h), \\ \left\langle \frac{\tilde{\theta}^m - \tilde{\theta}^{m-1}}{\tau}, \tilde{v}_h \right\rangle + \delta_w \langle \tilde{\theta}_x^m, \tilde{v}_{x,h} \rangle \\ = \langle \mathcal{C}_w(z^m, w^m) - \mathcal{C}_w(z_h^m, w_h^m), \tilde{v}_h \rangle + \tilde{R}^m(\tilde{v}_h), \end{aligned}$$

where

$$\begin{aligned} R^m(v_h) &= \left\langle \partial_t z(t^m) - \frac{\mathcal{P}_h z(t^m) - \mathcal{P}_h z(t^{m-1})}{\tau}, v_h \right\rangle, \\ \tilde{R}^m(\tilde{v}_h) &= \left\langle \partial_t w(t^m) - \frac{\mathcal{P}_h w(t^m) - \mathcal{P}_h w(t^{m-1})}{\tau}, \tilde{v}_h \right\rangle. \end{aligned}$$

Setting $v_h = \hat{\theta}^m$ and $\tilde{v}_h = \tilde{\theta}^m$, respectively, and simplifying

$$\begin{aligned} \langle \hat{\theta}^m, \hat{\theta}^m \rangle + \tau\delta_z \langle \hat{\theta}_x^m, \hat{\theta}_x^m \rangle &= \langle \hat{\theta}^{m-1}, \hat{\theta}^m \rangle \\ &\quad + \tau \langle \mathcal{C}_z(z^m, w^m) - \mathcal{C}_z(z_h^m, w_h^m), \hat{\theta}^m \rangle + \tau R^m(\hat{\theta}^m), \\ \langle \tilde{\theta}^m, \tilde{\theta}^m \rangle + \tau\delta_w \langle \tilde{\theta}_x^m, \tilde{\theta}_x^m \rangle &= \langle \tilde{\theta}^{m-1}, \tilde{\theta}^m \rangle \\ &\quad + \tau \langle \mathcal{C}_w(z^m, w^m) - \mathcal{C}_w(z_h^m, w_h^m), \tilde{\theta}^m \rangle + \tau \tilde{R}^m(\tilde{\theta}^m), \end{aligned}$$

thus,

$$\begin{aligned} \|\hat{\theta}^m\|_{\mathcal{L}^2}^2 + \tau\delta_z \|\hat{\theta}_x^m\|_{\mathcal{L}^2}^2 &= \langle \hat{\theta}^{m-1}, \hat{\theta}^m \rangle \\ &\quad + \tau \langle \mathcal{C}_z(z^m, w^m) - \mathcal{C}_z(z_h^m, w_h^m), \hat{\theta}^m \rangle + \tau R^m(\hat{\theta}^m), \end{aligned} \tag{22}$$

$$\begin{aligned} \|\check{\theta}^m\|_{\mathcal{L}^2}^2 + \tau \delta_w \|\check{\theta}_x^m\|_{\mathcal{L}^2}^2 &= \langle \check{\theta}^{m-1}, \check{\theta}^m \rangle \\ &+ \tau \langle \mathcal{C}_w(z^m, w^m) - \mathcal{C}_w(z_h^m, w_h^m), \check{\theta}^m \rangle + \tau \check{R}^m(\check{\theta}^m). \end{aligned} \quad (23)$$

The nonlinear term of (22) can be bounded by setting $\varepsilon^m = \hat{\theta}^m$ in (17), applying a similar process, and simplifying, so we finally obtain

$$\begin{aligned} &\left| \langle \mathcal{C}_z(z^m, w^m) - \mathcal{C}_z(z_h^m, w_h^m), \hat{\theta}^m \rangle \right| \\ &\leq C \left(\|\hat{\theta}^m\|_{\mathcal{L}^2}^2 + \|\check{\theta}^m\|_{\mathcal{L}^2}^2 + h^4 \right). \end{aligned} \quad (24)$$

For the residual $R^m(\hat{\theta}^m)$, we have

$$R^m(\hat{\theta}^m) = \left\langle \partial_t z(t^m) - \frac{\mathcal{P}_h z(t^m) - \mathcal{P}_h z(t^{m-1})}{\tau}, \hat{\theta}^m \right\rangle,$$

applying Cauchy-Schwartz inequality

$$R^m(\hat{\theta}^m) \leq \left\| \partial_t z(t^m) - \frac{\mathcal{P}_h z(t^m) - \mathcal{P}_h z(t^{m-1})}{\tau} \right\|_{\mathcal{L}^2} \|\hat{\theta}^m\|_{\mathcal{L}^2}.$$

The first term on the right-hand side of last inequality can be expressed as

$$\partial_t z(t^m) - \frac{\mathcal{P}_h z(t^m) - \mathcal{P}_h z(t^{m-1})}{\tau} = \vartheta_{time} + \vartheta_{space},$$

where, ϑ_{time} is the error of the temporal discretization

$$\vartheta_{time} = \mathcal{P}_h \left(\partial_t z(t^m) - \frac{z(t^m) - z(t^{m-1})}{\tau} \right),$$

and ϑ_{space} is the spatial discretization error

$$\vartheta_{space} = (\partial_t z(t^m) - \mathcal{P}_h \partial_t z(t^m)).$$

To estimate ϑ_{time} , we recruit the Taylor expansion to expand $z(t^{m-1})$ around t^m such that, for some $\xi^m \in [t^{m-1}, t^m]$, we have

$$z(t^{m-1}) = z(t^m - \tau) \approx z(t^m) - \tau \partial_t z(t^m) + \frac{\tau^2}{2} \partial_{tt} z(\xi^m),$$

these imply that

$$\frac{z(t^m) - z(t^{m-1})}{\tau} \approx \partial_t z(t^m) - \frac{\tau}{2} \partial_{tt} z(\xi^m),$$

thus,

$$\partial_t z(t^m) - \frac{z(t^m) - z(t^{m-1})}{\tau} \approx \frac{\tau}{2} \partial_{tt} z(\xi^m),$$

take the norm, we obtain

$$\left\| \partial_t z(t^m) - \frac{z(t^m) - z(t^{m-1})}{\tau} \right\|_{\mathcal{L}^2} \leq C\tau.$$

Using the \mathcal{L}^2 -stability of \mathcal{P}_h (projection stability)

$$\begin{aligned} \|\vartheta_{time}\|_{\mathcal{L}^2} &= \left\| \mathcal{P}_h \left(\partial_t z(t^m) - \frac{z(t^m) - z(t^{m-1})}{\tau} \right) \right\|_{\mathcal{L}^2} \\ &\leq C \left\| \partial_t z(t^m) - \frac{z(t^m) - z(t^{m-1})}{\tau} \right\|_{\mathcal{L}^2} \\ &\leq C\tau. \end{aligned}$$

Now, to estimate the special discretization error (projection error), we assume that $\partial_t z(t^m) \in \mathcal{H}^{r+1}(\mathcal{D})$, thus

$$\begin{aligned} \|\vartheta_{space}\|_{\mathcal{L}^2} &= \|\partial_t z(t^m) - \mathcal{P}_h \partial_t z(t^m)\|_{\mathcal{L}^2} \\ &\leq Ch^{r+1} \|\partial_t z(t^m)\|_{\mathcal{H}^{r+1}} \leq Ch^{r+1}. \end{aligned}$$

Selecting $r = 1$, applying the triangular inequality, and substituting the two estimates of ϑ_{time} and ϑ_{space} yields

$$\begin{aligned} \left\| \partial_t z(t^m) - \frac{\mathcal{P}_h z(t^m) - \mathcal{P}_h z(t^{m-1})}{\tau} \right\|_{\mathcal{L}^2} \\ \leq \|\vartheta_{time}\|_{\mathcal{L}^2} + \|\vartheta_{space}\|_{\mathcal{L}^2} \leq C\tau + Ch^2, \end{aligned}$$

by the aid of the parabolic CFL condition, we can take $\tau \sim h^2$, thus arranging the terms, we conclude that

$$\left\| \partial_t z(t^m) - \frac{\mathcal{P}_h z(t^m) - \mathcal{P}_h z(t^{m-1})}{\tau} \right\|_{\mathcal{L}^2} \leq Ch^2,$$

consequently, using the Young's inequality we obtain

$$\begin{aligned} R^m(\hat{\theta}^m) &\leq \left\| \partial_t z(t^m) - \frac{\mathcal{P}_h z(t^m) - \mathcal{P}_h z(t^{m-1})}{\tau} \right\|_{\mathcal{L}^2} \|\hat{\theta}^m\|_{\mathcal{L}^2} \\ &\leq Ch^2 \|\hat{\theta}^m\|_{\mathcal{L}^2} \\ &\leq C \left(h^4 + \|\hat{\theta}^m\|_{\mathcal{L}^2}^2 \right) \end{aligned} \quad (25)$$

Substituting estimates (24) and (25) into (22), applying the Cauchy-Schwartz and Young's inequality yields

$$\begin{aligned} \frac{1}{2\tau} \left(\|\hat{\theta}^m\|_{\mathcal{L}^2}^2 - \|\hat{\theta}^{m-1}\|_{\mathcal{L}^2}^2 \right) + \delta_z \|\hat{\theta}_x^m\|_{\mathcal{L}^2}^2 \\ \leq C \left(\|\hat{\theta}^m\|_{\mathcal{L}^2}^2 + \|\check{\theta}^m\|_{\mathcal{L}^2}^2 + h^4 \right). \end{aligned}$$

A similar analysis is applied on (23) to get

$$\begin{aligned} \frac{1}{2\tau} \left(\|\check{\theta}^m\|_{\mathcal{L}^2}^2 - \|\check{\theta}^{m-1}\|_{\mathcal{L}^2}^2 \right) + \delta_z \|\check{\theta}_x^m\|_{\mathcal{L}^2}^2 \\ \leq C \left(\|\hat{\theta}^m\|_{\mathcal{L}^2}^2 + \|\check{\theta}^m\|_{\mathcal{L}^2}^2 + h^4 \right). \end{aligned}$$

Adding the previous two inequalities

$$\begin{aligned} \frac{1}{2\tau} \left(\|\hat{\theta}^m\|_{\mathcal{L}^2}^2 + \|\check{\theta}^m\|_{\mathcal{L}^2}^2 - \|\hat{\theta}^{m-1}\|_{\mathcal{L}^2}^2 - \|\check{\theta}^{m-1}\|_{\mathcal{L}^2}^2 \right) \\ + \check{C} \left(\|\hat{\theta}_x^m\|_{\mathcal{L}^2}^2 + \|\check{\theta}_x^m\|_{\mathcal{L}^2}^2 \right) \\ \leq C \left(\|\hat{\theta}^m\|_{\mathcal{L}^2}^2 + \|\check{\theta}^m\|_{\mathcal{L}^2}^2 + h^4 \right), \end{aligned}$$

since $\|\hat{\theta}_x^m\|_{\mathcal{L}^2}^2 \geq 0$ and $\|\check{\theta}_x^m\|_{\mathcal{L}^2}^2 \geq 0$, then

$$\begin{aligned} & \frac{1}{2\tau} \left(\|\hat{\theta}^m\|_{\mathcal{L}^2}^2 + \|\check{\theta}^m\|_{\mathcal{L}^2}^2 - \|\hat{\theta}^{m-1}\|_{\mathcal{L}^2}^2 - \|\check{\theta}^{m-1}\|_{\mathcal{L}^2}^2 \right) \\ & \leq C \left(\|\hat{\theta}^m\|_{\mathcal{L}^2}^2 + \|\check{\theta}^m\|_{\mathcal{L}^2}^2 + h^4 \right), \end{aligned}$$

multiplying by 2τ and rearranging yields

$$\begin{aligned} & (1 - 2\tau C) \left(\|\hat{\theta}^m\|_{\mathcal{L}^2}^2 + \|\check{\theta}^m\|_{\mathcal{L}^2}^2 \right) \\ & \leq \left(\|\hat{\theta}^{m-1}\|_{\mathcal{L}^2}^2 + \|\check{\theta}^{m-1}\|_{\mathcal{L}^2}^2 \right) + 2\tau C h^4, \end{aligned}$$

assuming τ is sufficiently small, then $1 - 2\tau C \geq 0$, an so we have

$$\mathcal{E}^m \leq \frac{1}{1 - 2\tau C} \mathcal{E}^{m-1} + \frac{2\tau C}{1 - 2\tau C} h^4,$$

where

$$\mathcal{E}^m = \|\hat{\theta}^m\|_{\mathcal{L}^2}^2 + \|\check{\theta}^m\|_{\mathcal{L}^2}^2, \quad \mathcal{E}^{m-1} = \|\hat{\theta}^{m-1}\|_{\mathcal{L}^2}^2 + \|\check{\theta}^{m-1}\|_{\mathcal{L}^2}^2,$$

thus, by recursion we obtain

$$\mathcal{E}^m \leq \left(\frac{1}{1 - 2\tau C} \right)^m \mathcal{E}^0 + \left(\frac{2\tau C}{1 - 2\tau C} \right) h^4 \sum_{k=0}^{m-1} \left(\frac{1}{1 - 2\tau C} \right)^k,$$

by the aid of discrete Grönwall's lemma we can reach to

$$\begin{aligned} \max_{0 \leq m \leq M} \left(\|\hat{\theta}^m\|_{\mathcal{L}^2}^2 + \|\check{\theta}^m\|_{\mathcal{L}^2}^2 \right) &= \max_{0 \leq m \leq M} (\mathcal{E}^m) \\ &\leq C (\tau^2 + h^4). \end{aligned} \tag{26}$$

Also, from the theory of elliptic projection, we have

$$\max_{0 \leq m \leq M} \|\hat{\eta}^m\|_{\mathcal{L}^2} \leq C h^2, \quad \max_{0 \leq m \leq M} \|\check{\eta}^m\|_{\mathcal{L}^2} \leq C h^2. \tag{27}$$

Combining all derived estimates (26) and (27), taking the square root and simplifying, the proof is accomplished. \square

4 Computational Framework

In this section, we describe the computational methodology adopted for simulating the GSM using the finite element method in combination with the backward Euler time discretization scheme. The numerical framework was implemented in MATLAB, leveraging its matrix-oriented environment and built-in numerical solvers to efficiently handle system assembly and time evolution. We detail the construction of the mass and stiffness matrices, the treatment of nonlinear terms. The implementation was designed to be flexible and extensible, making it suitable for further investigations of complex pattern-forming systems.

From (7) and (8), we have

$$z_h^m(x, t) = \sum_{j=1}^N Z_j^m(t) \varphi_j(x), \tag{28}$$

$$w_h^m(x, t) = \sum_{j=1}^N W_j^m(t) \varphi_j(x). \tag{29}$$

Setting $v_h, \check{v}_h = \varphi_k, \forall v_h \in \mathcal{V}^h, k = 1, 2, \dots, N$, substituting (28) and (29) into (9), (10), yields

$$\begin{aligned} & \left\langle \sum_{j=1}^N Z_j^m \varphi_j, \varphi_k \right\rangle + \tau \mathfrak{B} \left(\sum_{j=1}^N Z_j^m \varphi_j, \varphi_k \right) \\ &= \left\langle \sum_{j=1}^N Z_j^{m-1} \varphi_j, \varphi_k \right\rangle \\ &+ \tau \left\langle \mathcal{C}_z \left(\sum_{j=1}^N Z_j^m \varphi_j, \sum_{j=1}^N W_j^m \varphi_j \right), \varphi_k \right\rangle, \end{aligned}$$

$$\begin{aligned} & \left\langle \sum_{j=1}^N W_j^m \varphi_j, \varphi_k \right\rangle + \tau \mathfrak{B} \left(\sum_{j=1}^N W_j^m \varphi_j, \varphi_k \right) \\ &= \left\langle \sum_{j=1}^N W_j^{m-1} \varphi_j, \varphi_k \right\rangle \\ &+ \tau \left\langle \mathcal{C}_w \left(\sum_{j=1}^N Z_j^m \varphi_j, \sum_{j=1}^N W_j^m \varphi_j \right), \varphi_k \right\rangle, \end{aligned}$$

thus, recalling the functions \mathcal{C}_z and \mathcal{C}_w with some mathematical manipulation we obtain

$$\begin{aligned} & \left\langle \sum_{j=1}^N Z_j^m \varphi_j, \varphi_k \right\rangle + \tau \delta_z \left\langle \sum_{j=1}^N Z_j^m \varphi_{x,j}, \varphi_{x,k} \right\rangle \\ &= \left\langle \sum_{j=1}^N Z_j^{m-1} \varphi_j, \varphi_k \right\rangle + \tau \alpha \left\langle \left(1 - \sum_{j=1}^N Z_j^m \varphi_k \right), \varphi_k \right\rangle \\ &- \tau \left\langle \left(\sum_{j=1}^N Z_j^m \varphi_k \right) \left(\sum_{j=1}^N W_j^m \varphi_k \right)^2, \varphi_k \right\rangle, \end{aligned}$$

$$\begin{aligned} & \left\langle \sum_{j=1}^N W_j^m \varphi_j, \varphi_k \right\rangle + \tau \delta_w \left\langle \sum_{j=1}^N W_j^m \varphi_{x,j}, \varphi_{x,k} \right\rangle \\ &= \left\langle \sum_{j=1}^N W_j^{m-1} \varphi_j, \varphi_k \right\rangle - \tau \beta \left\langle \sum_{j=1}^N W_j^m \varphi_j, \varphi_k \right\rangle \\ &+ \tau \left\langle \left(\sum_{j=1}^N Z_j^m \varphi_k \right) \left(\sum_{j=1}^N W_j^m \varphi_k \right)^2, \varphi_k \right\rangle, \end{aligned}$$

therefore, for uniform temporal discretization step size τ and spatial step length $h = x_{i+1} - x_i$, we can rewrite the above two equations for one generic element $e_i = (x_i, x_{i+1})$ and for

$k = i, i + 1$ as

$$\begin{aligned} & \sum_{j=i}^{i+1} Z_j^m \langle \varphi_j, \varphi_k \rangle + \tau \delta_z \sum_{j=i}^{i+1} Z_j^m \langle \varphi_{x,j}, \varphi_{x,k} \rangle \\ &= \sum_{j=i}^{i+1} Z_j^{m-1} \langle \varphi_j, \varphi_k \rangle + \tau \langle \alpha, \varphi_k \rangle - \tau \alpha \sum_{j=i}^{i+1} Z_j^m \langle \varphi_j, \varphi_k \rangle \\ & \quad - \tau \left\langle \left(\sum_{j=i}^{i+1} Z_j^m \varphi_k \right) \left(\sum_{j=i}^{i+1} W_j^m \varphi_k \right)^2, \varphi_k \right\rangle, \end{aligned}$$

$$\begin{aligned} & \sum_{j=i}^{i+1} W_j^m \langle \varphi_j, \varphi_k \rangle + \tau \delta_w \sum_{j=i}^{i+1} W_j^m \langle \varphi_{x,j}, \varphi_{x,k} \rangle \\ &= \sum_{j=i}^{i+1} W_j^{m-1} \langle \varphi_j, \varphi_k \rangle - \tau \beta \sum_{j=i}^{i+1} W_j^m \langle \varphi_j, \varphi_k \rangle \\ & \quad + \tau \left\langle \left(\sum_{j=i}^{i+1} Z_j^m \varphi_k \right) \left(\sum_{j=i}^{i+1} W_j^m \varphi_k \right)^2, \varphi_k \right\rangle, \end{aligned}$$

these implies that:

$$\mathbf{A}Z^m = \mathbf{F}_z (Z^{m-1}) \quad (30)$$

$$\mathbf{B}W^m = \mathbf{F}_w (W^{m-1}) \quad (31)$$

where

$$\mathbf{A} = M + \tau \delta_z S + \tau \alpha M + \tau G_z,$$

$$\mathbf{B} = M + \tau \delta_w S + \tau \beta M - \tau G_w,$$

$$\mathbf{F}_z (Z^{m-1}) = \frac{\tau \alpha h}{2} O + \tau M Z^{m-1},$$

$$\mathbf{F}_w (W^{m-1}) = \tau M W^{m-1},$$

M and S symbolize the mass and stiffness matrices, which are assembled from element matrices M^e and S^e , where

$$M^e = \langle \varphi_j, \varphi_k \rangle = \int_{x_i}^{x_{i+1}} \varphi_j \cdot \varphi_k dx = \frac{h}{6} \begin{bmatrix} 2 & 1 \\ 1 & 2 \end{bmatrix},$$

$$S^e = \langle \varphi_{x,j}, \varphi_{x,k} \rangle = \int_{x_i}^{x_{i+1}} \frac{\partial \varphi_j}{\partial x} \cdot \frac{\partial \varphi_k}{\partial x} dx = \frac{1}{h} \begin{bmatrix} 1 & -1 \\ -1 & 1 \end{bmatrix},$$

also, O is the matrix that assembled from

$$O^e = \begin{bmatrix} 1 \\ 1 \end{bmatrix},$$

Finally, the two matrices G_z and G_w are assembled from G_z^e and G_w^e which are produced from the inner product of the nonlinear term, occurring in the system after extracting the approximated solutions Z^m and W^m . Because of the complexity of this process, it will be treated specifically in detail through a forthcoming lemma.

Lemma 4.1. *Suppose a uniform spatial and temporal discretization for the domain $(0, T] \times \mathfrak{D}$, then, the inner product of the nonlinear term can be written as*

$$\left\langle \left(\sum_{j=i}^{i+1} Z_j^m \varphi_k \right) \left(\sum_{j=i}^{i+1} W_j^m \varphi_k \right)^2, \varphi_k \right\rangle = G_z^e Z^m \quad (32)$$

and

$$\left\langle \left(\sum_{j=i}^{i+1} Z_j^m \varphi_k \right) \left(\sum_{j=i}^{i+1} W_j^m \varphi_k \right)^2, \varphi_k \right\rangle = G_w^e W^m \quad (33)$$

where

$$Z^m = \begin{bmatrix} Z_i^m \\ Z_{i+1}^m \end{bmatrix}, \quad W^m = \begin{bmatrix} W_i^m \\ W_{i+1}^m \end{bmatrix}$$

and

$$G_z^e = \frac{h}{60} \begin{bmatrix} b_1 & b_2 \\ b_2 & b_3 \end{bmatrix}, \quad G_w^e = \frac{h}{60} \begin{bmatrix} d_1 & d_2 \\ d_2 & d_3 \end{bmatrix},$$

with

$$b_1 = 12 (W_i^m)^2 + 6 W_i^m W_{i+1}^m + 2 (W_{i+1}^m)^2,$$

$$b_2 = 3 (W_i^m)^2 + 4 W_i^m W_{i+1}^m + 3 (W_{i+1}^m)^2,$$

$$b_3 = 2 (W_i^m)^2 + 6 W_i^m W_{i+1}^m + 12 (W_{i+1}^m)^2,$$

and

$$d_1 = (12 Z_i^m + 3 Z_{i+1}^m) W_i^m + (3 Z_i^m + 2 Z_{i+1}^m) W_{i+1}^m,$$

$$d_2 = (3 Z_i^m + 2 Z_{i+1}^m) W_i^m + (2 Z_i^m + 3 Z_{i+1}^m) W_{i+1}^m,$$

$$d_3 = (2 Z_i^m + 3 Z_{i+1}^m) W_i^m + (3 Z_i^m + 12 Z_{i+1}^m) W_{i+1}^m.$$

Proof. From definition of the inner product $\langle \cdot, \cdot \rangle$ and for one element we have

$$\begin{aligned} & \left\langle \left(\sum_{j=i}^{i+1} Z_j^m \varphi_j \right) \left(\sum_{j=i}^{i+1} W_j^m \varphi_j \right)^2, \varphi_k \right\rangle \\ &= \int_{x_i}^{x_{i+1}} \left(\sum_{j=i}^{i+1} W_j^m \varphi_j \right)^2 \left(\sum_{j=i}^{i+1} Z_j^m \varphi_j \right) \varphi_k dx \\ &= \sum_{j=i}^{i+1} Z_j^m \int_{x_i}^{x_{i+1}} \left(\sum_{j=i}^{i+1} W_j^m \varphi_j \right)^2 \varphi_j \varphi_k dx \\ &= \sum_{j=i}^{i+1} Z_j^m \int_{x_i}^{x_{i+1}} (W_i^m \varphi_i + W_{i+1}^m \varphi_{i+1})^2 \varphi_j \varphi_k dx \\ &= \sum_{j=i}^{i+1} Z_j^m \int_{x_i}^{x_{i+1}} \left((W_i^m)^2 \varphi_i^2 + 2 W_i^m \varphi_i W_{i+1}^m \varphi_{i+1} \right. \\ & \quad \left. + (W_{i+1}^m)^2 \varphi_{i+1}^2 \right) \varphi_j \varphi_k dx \\ &= \sum_{j=i}^{i+1} Z_j^m (W_i^m)^2 \int_{x_i}^{x_{i+1}} \varphi_i^2 \varphi_j \varphi_k dx \\ & \quad + 2 \sum_{j=i}^{i+1} Z_j^m W_i^m W_{i+1}^m \int_{x_i}^{x_{i+1}} \varphi_i \varphi_{i+1} \varphi_j \varphi_k dx \\ & \quad + \sum_{j=i}^{i+1} Z_j^m (W_{i+1}^m)^2 \int_{x_i}^{x_{i+1}} \varphi_{i+1}^2 \varphi_j \varphi_k dx. \end{aligned} \quad (34)$$

Consequently, the first term on RHS of Eq.(34) can be computed as follows:

$$\begin{aligned} \sum_{j=i}^{i+1} Z_j^m (W_i^m)^2 \int_{x_i}^{x_{i+1}} \varphi_i^2 \varphi_j \varphi_k dx \\ = Z_i^m (W_i^m)^2 \int_{x_i}^{x_{i+1}} \varphi_i^3 \varphi_k dx \\ + Z_{i+1}^m (W_i^m)^2 \int_{x_i}^{x_{i+1}} \varphi_i^2 \varphi_{i+1} \varphi_k dx. \end{aligned} \tag{35}$$

For $k = i$,

$$\begin{aligned} \int_{x_i}^{x_{i+1}} \varphi_i^3 \varphi_k dx &= \int_{x_i}^{x_{i+1}} \varphi_i^4 dx = \frac{12h}{60}, \\ \int_{x_i}^{x_{i+1}} \varphi_i^2 \varphi_{i+1} \varphi_k dx &= \int_{x_i}^{x_{i+1}} \varphi_i^3 \varphi_{i+1} dx = \frac{3h}{60}. \end{aligned}$$

substituting in (35) gives

$$\begin{aligned} \sum_{j=i}^{i+1} Z_j^m (W_i^m)^2 \int_{x_i}^{x_{i+1}} \varphi_i^2 \varphi_j \varphi_k dx \\ = \frac{12h}{60} Z_i^m (W_i^m)^2 + \frac{3h}{60} Z_{i+1}^m (W_i^m)^2. \end{aligned} \tag{36}$$

For $k = i + 1$,

$$\begin{aligned} \int_{x_i}^{x_{i+1}} \varphi_i^3 \varphi_k dx &= \int_{x_i}^{x_{i+1}} \varphi_i^3 \varphi_{i+1} dx = \frac{3h}{60}, \\ \int_{x_i}^{x_{i+1}} \varphi_i^2 \varphi_{i+1} \varphi_k dx &= \int_{x_i}^{x_{i+1}} \varphi_i^2 \varphi_{i+1}^2 dx = \frac{2h}{60}. \end{aligned}$$

thus,

$$\begin{aligned} \sum_{j=i}^{i+1} Z_j^m (W_i^m)^2 \int_{x_i}^{x_{i+1}} \varphi_i^2 \varphi_j \varphi_k dx \\ = \frac{3h}{60} Z_i^m (W_i^m)^2 + \frac{2h}{60} Z_{i+1}^m (W_i^m)^2. \end{aligned} \tag{37}$$

By combining (36) and (37), the first term on RHS of (34) can be constructed as the following vector:

$$\begin{aligned} \Upsilon_1 &= \sum_{j=i}^{i+1} Z_j^m (W_i^m)^2 \int_{x_i}^{x_{i+1}} \varphi_i^2 \varphi_j \varphi_k dx \\ &= \begin{bmatrix} \frac{12h}{60} Z_i^m (W_i^m)^2 + \frac{3h}{60} Z_{i+1}^m (W_i^m)^2 \\ \frac{3h}{60} Z_i^m (W_i^m)^2 + \frac{2h}{60} Z_{i+1}^m (W_i^m)^2 \end{bmatrix}, \end{aligned}$$

which can be expressed as

$$\begin{aligned} \Upsilon_1 &= \begin{bmatrix} \frac{12h}{60} Z_i^m (W_i^m)^2 + \frac{3h}{60} Z_{i+1}^m (W_i^m)^2 \\ \frac{3h}{60} Z_i^m (W_i^m)^2 + \frac{2h}{60} Z_{i+1}^m (W_i^m)^2 \end{bmatrix} \\ &= \frac{h}{60} \begin{bmatrix} 12(W_i^m)^2 & 3(W_i^m)^2 \\ 3(W_i^m)^2 & 2(W_i^m)^2 \end{bmatrix} \begin{bmatrix} Z_i^m \\ Z_{i+1}^m \end{bmatrix}. \end{aligned}$$

Similar calculations will obtain Υ_2 and Υ_3 for the second and third terms on the RHS of (34), respectively, where

$$\begin{aligned} \Upsilon_2 &= \frac{h}{60} \begin{bmatrix} 6W_i W_{i+1} & 4W_i W_{i+1} \\ 4W_i W_{i+1} & 6W_i W_{i+1} \end{bmatrix} \begin{bmatrix} Z_i^m \\ Z_{i+1}^m \end{bmatrix}, \\ \Upsilon_3 &= \frac{h}{60} \begin{bmatrix} 2W_{i+1}^2 & 3W_{i+1}^2 \\ 3W_{i+1}^2 & 12W_{i+1}^2 \end{bmatrix} \begin{bmatrix} Z_i^m \\ Z_{i+1}^m \end{bmatrix}. \end{aligned}$$

Substituting $\Upsilon_1, \Upsilon_2, \Upsilon_3$ in (34) and simplified yields the inner product (32).

A similar fashion can be applied to obtain Eq.(33), which accomplishes the proof. \square

5 Numerical Results

This section presents the effectiveness of the proposed numerical scheme through the application to two test cases. All results were generated using MATLAB R2024a on a Lenovo laptop (Intel Core i7 13th gen. processor, integrated with 16 GB RAM, running Windows 11 OS). To evaluate the accuracy of the suggested scheme, we computed errors in \mathcal{L}^2 and \mathcal{L}^∞ norms with the absolute error, which uses data measurements to evaluate the difference between the approximated and theoretical results, where the absolute error \mathcal{E} is identified by

$$\begin{aligned} \mathcal{E}_z &= |z - z_h| = |z_{exact} - z_{app}|, \\ \mathcal{E}_w &= |w - w_h| = |w_{exact} - w_{app}|, \end{aligned}$$

the error of the \mathcal{L}^2 - norm, symbolized by $(\hat{\mathcal{E}}_{\mathcal{L}^2})$, is

$$\mathcal{E}_{\mathcal{L}^2}(z) = \|z - z_h\|_{\mathcal{L}^2} = \sqrt{\sum_{j=0}^N \int_{x_j}^{x_{j+1}} (z(x, t) - z_h(x, t))^2 dx},$$

and the \mathcal{L}^∞ -norm error $(\hat{\mathcal{E}}_{\mathcal{L}^\infty})$ is

$$\mathcal{E}_{\mathcal{L}^\infty}(w) = \|z - z_h\|_{\mathcal{L}^\infty} = \max_{0 \leq j \leq N} |z(x_j, t) - z_h(x_j, t)|.$$

The spatial rate of convergence can be also defined in $\mathcal{E}_{\mathcal{L}^2}$ and $\mathcal{E}_{\mathcal{L}^\infty}$, respectively, as

$$RoC_S(\mathcal{E}_{\mathcal{L}^2}) = \frac{\log(\mathcal{E}_{\mathcal{L}^2}(h_1)/\mathcal{E}_{\mathcal{L}^2}(h_2))}{\log(h_1/h_2)},$$

$$RoC_S(\mathcal{E}_{\mathcal{L}^\infty}) = \frac{\log(\mathcal{E}_{\mathcal{L}^\infty}(h_1)/\mathcal{E}_{\mathcal{L}^\infty}(h_2))}{\log(h_1/h_2)},$$

and the temporal convergence rate in $\mathcal{E}_{\mathcal{L}^2}$ and $\mathcal{E}_{\mathcal{L}^\infty}$, as

$$RoC_T(\mathcal{E}_{\mathcal{L}^2}) = \frac{\log(\mathcal{E}_{\mathcal{L}^2}(\tau_1)/\mathcal{E}_{\mathcal{L}^2}(\tau_2))}{\log(\tau_1/\tau_2)},$$

$$RoC_T(\mathcal{E}_{\mathcal{L}^\infty}) = \frac{\log(\mathcal{E}_{\mathcal{L}^\infty}(\tau_1)/\mathcal{E}_{\mathcal{L}^\infty}(\tau_2))}{\log(\tau_1/\tau_2)}.$$

Example 5.1. Referring that the exact solution of (1) and (2) are given by:

$$z(x, t) = \frac{3 - \sqrt{a}}{4} - \frac{\sqrt{2b}}{4} \tanh\left(\frac{\sqrt{b}}{4} - (x - ct)\right),$$

$$w(x, t) = \frac{1 + \sqrt{a}}{4} + \frac{\sqrt{2b}}{4} \tanh\left(\frac{\sqrt{b}}{4} - (x - ct)\right),$$

where

$$a = 1 - 4\alpha, \quad b = 1 + \sqrt{a} - 2\alpha, \quad c = \frac{\sqrt{2}(1 - 3\sqrt{a})}{4},$$

with initial conditions

$$z(x, 0) = \frac{3 - \sqrt{a}}{4} - \frac{\sqrt{2b}}{4} \tanh\left(\frac{\sqrt{b}}{4} - x\right),$$

$$w(x, 0) = \frac{1 + \sqrt{a}}{4} + \frac{\sqrt{2b}}{4} \tanh\left(\frac{\sqrt{b}}{4} - x\right),$$

and homogeneous Neumann boundary conditions

$$\frac{\partial z}{\partial x} = 0, \quad \frac{\partial w}{\partial x} = 0.$$

For spatial and temporal discretization, we chose $L = 30$, $N = 121$, $h = 0.5$ and $\tau = \Delta t = 0.001$, total time $T = 1$, $\alpha = \beta = 0.218$ and $\delta_z = \delta_w = 1$. Figures and calculated data tables are shown to demonstrate the behavior of the FE solutions compared with the exact solution, highlighting the discretization impact of time and space.

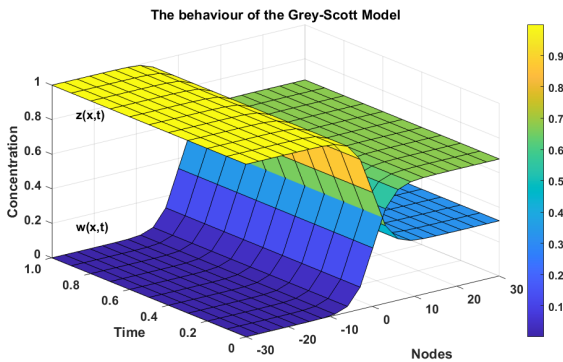


Figure 1. The behavior of the GSM solutions for Example5.1.

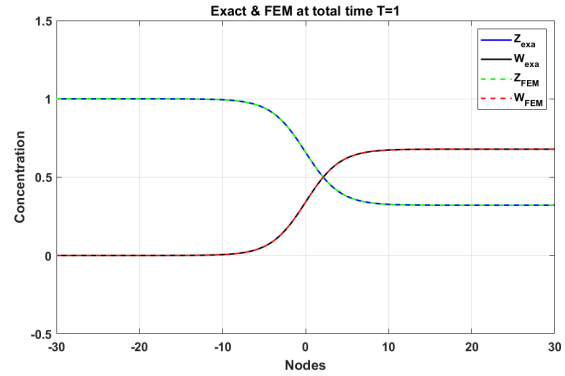


Figure 2. Comparison between the exact and approximate solutions for Example5.1.

Table 1. Comparison between the exact(z) and approximate(z) solutions with the absolute error estimation \mathcal{E}_z at some selected nodes for Example5.1.

$N = 121, \tau = \Delta t = 0.001, T = 1, L = 30$ $\delta_z = \delta_w = 1, \alpha = \beta = 0.218$			
x	Exact(z)	Approximate(z)	\mathcal{E}_z
-30.0	9.999996e-01	9.999996e-01	4.731466e-09
-25.0	9.999958e-01	9.999958e-01	5.216680e-08
-20.0	9.999535e-01	9.999541e-01	5.751006e-07
-15.0	9.994875e-01	9.994939e-01	6.332198e-06
-10.0	9.943922e-01	9.944610e-01	6.877799e-05
-5.0	9.428994e-01	9.435468e-01	6.473696e-04
0.0	6.584455e-01	6.605573e-01	2.111768e-03
5.0	3.769271e-01	3.775678e-01	6.406890e-04
10.0	3.265856e-01	3.266536e-01	6.794131e-05
15.0	3.216144e-01	3.216207e-01	6.254013e-06
20.0	3.211599e-01	3.211605e-01	5.679901e-07
25.0	3.211187e-01	3.211187e-01	5.152174e-08
30.0	3.211149e-01	3.211149e-01	4.672959e-09

Table 2. Comparison between the exact(w) and approximate(w) solutions with the absolute error estimation \mathcal{E}_w at some selected nodes for Example5.1.

$N = 121, \tau = \Delta t = 0.001, T = 1, L = 30$ $\delta_z = \delta_w = 1, \alpha = \beta = 0.218$			
x	Exact(w)	Approximate(w)	\mathcal{E}_w
-30.0	3.826307e-07	3.778992e-07	4.731466e-09
-25.0	4.218720e-06	4.166553e-06	5.216680e-08
-20.0	4.651114e-05	4.593604e-05	5.751006e-07
-15.0	5.124626e-04	5.061304e-04	6.332198e-06
-10.0	5.607784e-03	5.539006e-03	6.877799e-05
-5.0	5.710059e-02	5.645322e-02	6.473696e-04
0.0	3.415545e-01	3.394427e-01	2.111768e-03
5.0	6.230729e-01	6.224322e-01	6.406890e-04
10.0	6.734144e-01	6.733464e-01	6.794131e-05
15.0	6.783856e-01	6.783793e-01	6.254013e-06
20.0	6.788401e-01	6.788395e-01	5.679901e-07
25.0	6.788813e-01	6.788813e-01	5.152174e-08
30.0	6.788851e-01	6.788851e-01	4.672958e-09

Table 3. The errors in \mathcal{L}^2 and \mathcal{L}^∞ norms ($\mathcal{E}_{\mathcal{L}^2}$ and $\mathcal{E}_{\mathcal{L}^\infty}$) at different time $0 < t < T$ for Example 5.1.

$N = 121, \tau = \Delta t = 0.001, T = 1, L = 30$ $\delta_z = \delta_w = 1, \alpha = \beta = 0.218$				
time (t)	$\mathcal{E}_{\mathcal{L}^2}(z)$	$\mathcal{E}_{\mathcal{L}^2}(w)$	$\mathcal{E}_{\mathcal{L}^\infty}(z)$	$\mathcal{E}_{\mathcal{L}^\infty}(w)$
0.2	3.98037e-03	3.98004e-03	1.68860e-03	1.68846e-03
0.4	2.98348e-03	2.98284e-03	1.26546e-03	1.26519e-03
0.6	1.98673e-03	1.98580e-03	8.42334e-04	8.41943e-04
0.8	9.90592e-04	9.89385e-04	4.19228e-04	4.18721e-04
1.0	6.10034e-05	6.15493e-05	2.14433e-05	2.17979e-05

Table 4. The effect of spatial step-size h on z for Example 5.1.

$N = 121, T = 1, L = 30, \delta_z = \delta_w = 1, \alpha = \beta = 0.218$				
h	$\mathcal{E}_{\mathcal{L}^2}(z)$	$\mathcal{RoC}_S(\mathcal{E}_{\mathcal{L}^2})$	$\mathcal{E}_{\mathcal{L}^\infty}(z)$	$\mathcal{RoC}_S(\mathcal{E}_{\mathcal{L}^\infty})$
1/2	6.13892e-05		2.16388e-05	
1/4	1.53247e-05	2.0021	5.43736e-06	1.9926
1/8	3.82957e-06	2.0006	1.35670e-06	2.0028
1/16	9.69267e-07	1.9822	3.37015e-07	2.0092

Table 5. The effect of spatial step-size h on w for Example 5.1.

$N = 121, T = 1, L = 30, \delta_z = \delta_w = 1, \alpha = \beta = 0.218$				
h	$\mathcal{E}_{\mathcal{L}^2}(w)$	$\mathcal{RoC}_S(\mathcal{E}_{\mathcal{L}^2})$	$\mathcal{E}_{\mathcal{L}^\infty}(w)$	$\mathcal{RoC}_S(\mathcal{E}_{\mathcal{L}^\infty})$
1/2	6.13894e-05		2.16389e-05	
1/4	1.53248e-05	2.0021	5.43744e-06	1.9926
1/8	3.82970e-06	2.0006	1.35678e-06	2.0027
1/16	9.69393e-07	1.9821	3.37095e-07	2.0090

Table 6. The effect of temporal step-size τ on z for Example 5.1.

$N = 121, T = 1, L = 30, \delta_z = \delta_w = 1, \alpha = \beta = 0.218$				
τ	$\mathcal{E}_{\mathcal{L}^2}(z)$	$\mathcal{RoC}_S(\mathcal{E}_{\mathcal{L}^2})$	$\mathcal{E}_{\mathcal{L}^\infty}(z)$	$\mathcal{RoC}_S(\mathcal{E}_{\mathcal{L}^\infty})$
1/10	4.97750e-04		2.11189e-04	
1/20	2.48880e-04	1.0000	1.05597e-04	1.0000
1/40	1.24446e-04	0.9999	5.28014e-05	0.9999
1/80	6.22272e-05	0.9999	2.64031e-05	0.9999
1/160	3.11171e-05	0.9998	1.32018e-05	1.0000
1/320	1.55644e-05	0.9995	6.60404e-06	0.9993

Table 7. The effect of temporal step-size τ on w for Example 5.1.

$N = 121, T = 1, L = 30, \delta_z = \delta_w = 1, \alpha = \beta = 0.218$				
τ	$\mathcal{E}_{\mathcal{L}^2}(w)$	$\mathcal{RoC}_S(\mathcal{E}_{\mathcal{L}^2})$	$\mathcal{E}_{\mathcal{L}^\infty}(w)$	$\mathcal{RoC}_S(\mathcal{E}_{\mathcal{L}^\infty})$
1/10	4.97750e-04		2.11189e-04	
1/20	2.48879e-04	1.0000	1.05597e-04	1.0000
1/40	1.24445e-04	0.9999	5.28014e-05	0.9999
1/80	6.22271e-05	0.9999	2.64031e-05	0.9999
1/160	3.11300e-05	0.9992	1.32071e-05	0.9994
1/320	1.55676e-05	0.9998	6.60536e-06	0.9996

To consolidate the efficacy of the suggested scheme, we made a comparison with [30], setting $L = 20, N = 121$ and $\tau = \Delta t = 0.0001$, total time $T = 1, \alpha = \beta = 1/8$ and $\delta_z = \delta_w = 1$, the following results are obtained:

Table 8. Comparison of $\mathcal{E}_{\mathcal{L}^2}$ and $\mathcal{E}_{\mathcal{L}^\infty}$ between reference method [30] and proposed scheme of z for Example 5.1 at $N = 121$

$L = 20, \tau = 0.0001, \delta_z = \delta_w = 1, \alpha = \beta = \frac{1}{8}$				
time (t)	[30]		Proposed Scheme	
	$\mathcal{E}_{\mathcal{L}^2}(z)$	$\mathcal{E}_{\mathcal{L}^\infty}(z)$	$\mathcal{E}_{\mathcal{L}^2}(z)$	$\mathcal{E}_{\mathcal{L}^\infty}(z)$
0.2	7.7057e-05	9.2595e-05	4.30438e-05	2.39451e-05
0.4	6.1710e-05	6.8850e-05	7.54073e-05	4.15220e-05
0.6	4.3231e-04	4.3832e-04	1.06867e-04	5.80598e-05
0.8	8.1767e-04	7.7675e-04	1.37532e-04	7.38074e-05
1.0	7.2179e-04	6.7410e-04	1.67509e-04	8.89161e-05

Table 9. Comparison of $\mathcal{E}_{\mathcal{L}^2}$ and $\mathcal{E}_{\mathcal{L}^\infty}$ between reference method [30] and proposed scheme of w for Example 5.1 at $N = 121$

$L = 20, \tau = 0.0001, \delta_z = \delta_w = 1, \alpha = \beta = \frac{1}{8}$				
time (t)	[30]		Proposed Scheme	
	$\mathcal{E}_{\mathcal{L}^2}(w)$	$\mathcal{E}_{\mathcal{L}^\infty}(w)$	$\mathcal{E}_{\mathcal{L}^2}(w)$	$\mathcal{E}_{\mathcal{L}^\infty}(w)$
0.2	6.9334e-05	8.3661e-05	4.39172e-05	2.42817e-05
0.4	5.8902e-05	6.5661e-05	7.71060e-05	4.21951e-05
0.6	4.3144e-04	4.3616e-04	1.09370e-04	5.90674e-05
0.8	8.5434e-04	8.0607e-04	1.40818e-04	7.51462e-05
1.0	8.2662e-04	7.4450e-04	1.71554e-04	9.05820e-05

Choosing $N = 421$, and fixing other parameters, we obtained:

Table 10. Comparison of $\mathcal{E}_{\mathcal{L}^2}$ and $\mathcal{E}_{\mathcal{L}^\infty}$ between the reference method [30] and the proposed scheme of z for Example 5.1, at $N = 421$

$L = 20, \tau = 0.0001, \delta_z = \delta_w = 1, \alpha = \beta = \frac{1}{8}$				
time (t)	[30]		Proposed Scheme	
	$\mathcal{E}_{\mathcal{L}^2}(z)$	$\mathcal{E}_{\mathcal{L}^\infty}(z)$	$\mathcal{E}_{\mathcal{L}^2}(z)$	$\mathcal{E}_{\mathcal{L}^\infty}(z)$
0.2	1.0989e-04	8.4596e-05	1.23537e-05	6.15554e-06
0.4	7.6131e-04	4.7887e-04	1.41392e-05	7.23781e-06
0.6	8.7635e-04	5.0247e-04	1.60083e-05	8.28757e-06
0.8	0.0014	7.2644e-04	1.79274e-05	9.31002e-06
1.0	0.0018	9.7067e-04	1.98809e-05	1.03066e-05

Table 11. Comparison of $\mathcal{E}_{\mathcal{L}^2}$ and $\mathcal{E}_{\mathcal{L}^\infty}$ between reference method [30] and proposed scheme of w for Example 5.1 at $N = 421$

$L = 20, \tau = 0.0001, \delta_z = \delta_w = 1, \alpha = \beta = \frac{1}{8}$				
time (t)	[30]		Proposed Scheme	
	$\mathcal{E}_{\mathcal{L}^2}(w)$	$\mathcal{E}_{\mathcal{L}^\infty}(w)$	$\mathcal{E}_{\mathcal{L}^2}(w)$	$\mathcal{E}_{\mathcal{L}^\infty}(w)$
0.2	9.9243e-05	7.6701e-05	1.32577e-05	6.52745e-06
0.4	7.2577e-04	4.5632e-04	1.59103e-05	7.93973e-06
0.6	0.0011	6.2594e-04	1.86089e-05	9.30662e-06
0.8	9.0840e-04	4.8254e-04	2.13244e-05	1.06302e-05
1.0	0.0023	0.0011	2.40444e-05	1.19316e-05

The numerical results obtained in this study illustrate the precision and reliability of the suggested finite element approach for the one-dimensional GSM. Simulations validate that the fully discrete approach, using linear FE in spatial dimensions and backward Euler in temporal dimensions, accurately represents the intricate spatiotemporal dynamics of the system with great precision. The error norms calculated at different time levels, specifically the \mathcal{L}^2 and \mathcal{L}^∞ norms, exhibited a consistent decline with mesh refinement and time step reduction, hence confirming the stability and convergence of the system. The comparison between the approximated and exact solutions validates the capacity of the method to accurately simulate the dynamics, particularly in the presence of nonlinear coupling.

The results robustly validate the theoretical convergence analysis and illustrate the efficacy of the proposed computational approach in addressing the dynamics of the GSM.

Figure 1 depicts the behavior of the GSM for both z and v . The solution features and their associated meshes are produced with a uniform mesh. These provide a clear illustration of the physical behavior of the solution at multiple points.

Figure 2 shows a comparison between the exact and numerical approaches at the last iterated step, which equals 1000, given an interval $[-30,30]$ with equally spaced discretization. The figures also indicate that the FEM approximation is too close to the exact.

The numerical results given in Tables 1 and 2 provide the accuracy of the solution for the proposed scheme for the equations of z and w , respectively. The exact and FEM solutions, for some selected nodes, with their absolute errors are calculated, and the numerical solution coincides with the exact solution for good accuracy.

Table 3 investigates the influence of the temporal variable t on the accuracy of the approximated solution by evaluating the errors of the \mathcal{L}^2 and \mathcal{L}^∞ -norms. The results demonstrate that as time progresses, the numerical approximation improves in accuracy, leading to a noticeable reduction in the error values computed in both norms.

Tables 4 and 5 demonstrate the effects of the spatial step size h , whereas Tables 6 and 7 show the temporal step size τ . Errors in \mathcal{L}^2 and \mathcal{L}^∞ -norms are computed, along with the rate of convergence for both. These evaluations demonstrate that the numerical solution achieves the anticipated second-order accuracy in space and first-order accuracy in time, which is consistent with the theoretical expectations.

Finally, a comparison between our proposed scheme and that of [30] is presented in tables 8, 9, 10, and 11 at different times utilizing the errors in \mathcal{L}^2 and \mathcal{L}^∞ -norms, which show better results and consolidate the robustness of our scheme.

6 Conclusion and Future Work

In this study, we investigated a one-dimensional GSRDS using the GFEM. Starting from finding the weak formulation, we constructed a fully discrete scheme based on the Galerkin spatial discretization and backward Euler strategies. A complete convergence analysis was carried out by incorporating elliptic projection techniques, leading to optimal a priori error estimation in $\mathcal{L}^\infty(0, T; \mathcal{L}^2)$ -norms.

The numerical simulations supported the exact solutions, confirmed the theoretical rates of convergence and demonstrated the effectiveness of the proposed numerical schemes. Mesh and time-step refinement studies were also conducted to verify the temporal and spatial accuracy. This work lays a strong foundation for future studies on complex systems involving nonlinear reaction–diffusion dynamics. Potential extensions include higher-dimensional analysis, adaptive mesh refinement, and coupling with stochastic perturbations to model more realistic chemical and biological systems.

Acknowledgments

The authors would like to thank the Department of Mathematics, Faculty of Science and Health, Koya University, for their support.

Data Availability Statement

All data supporting the findings of this study are included within the article.

Conflict of Interest Statement

The authors declare that there are no conflicts of interest associated with this manuscript.

REFERENCES

- [1] M.A. Rasheed, S. Laverty, and B. Bannish, “Numerical solutions of a linear age-structured population model,” *AIP Conference Proceedings*, vol. 2096, no. 1, p. 020002, 2019, doi: 10.1063/1.5097799.
- [2] M. A. Rasheed and S. N. Kadhim, “Numerical solutions of two-dimensional vorticity transport equation using Crank–Nicolson method,” *Baghdad Science Journal*, vol. 19, no. 2, p. 23, 2022, doi: 10.21123/bsj.2022.19.2.0321.
- [3] M. A. Rasheed and F. N. Ghaffoori, “Numerical blow-up time and growth rate of a reaction–diffusion equation,” *Italian Journal of Pure and Applied Mathematics*, no. 44, pp. 805–813, 2020.
- [4] P. Gray and S.K. Scott, “Autocatalytic reactions in the isothermal, continuous stirred tank reactor: isolas and other forms of multistability,” *Chemical Engineering Science*, vol. 38, no. 1, pp. 29–43, 1983, doi: 10.1016/0009-2509(83)80132-8.
- [5] Y. A. Sabawi and H. Q. Hamad, “Numerical solution of the Whitham–Broer–Kaup shallow water equation by quartic B-spline collocation method,” *Physica Scripta*, vol. 99, no. 1, p. 015242, 2024, doi: 10.1088/1402-4896/ad1561.
- [6] O. T. Al-Bairaqdar, Y. A. Sabawi, and M. S. Hasso, “Efficient numerical solution of the Allen–Cahn equation via a non-lumping Galerkin finite element method,” *AIP Advances*, vol. 15, no. 7, 2025, doi: 10.1063/5.0262503.
- [7] Y. A. Sabawi and B. O. Hussien, “A cubic B-spline finite element method for Volterra integro-differential equation,” *Palestine Journal of Mathematics*, vol. 13, no. 3, pp. 571–583, 2024.
- [8] F. Dkhil, E. Logak and Y. Nishiura, “Some analytical results on the Gray–Scott model,” *Asymptotic Analysis*, vol. 39, no. (3–4), pp. 225–261, 2004, doi: 10.3233/ASY-2004-631.
- [9] A. Doelman, T.J. Kaper and P.A. Zegeling, “Pattern formation in the one-dimensional Gray–Scott model,” *Nonlinearity*, vol. 10, no. 2, p. 523, 1997, doi: 10.1088/0951-7715/10/2/013.

- [10] A. Doelman, R.A. Gardner and T.J. Kaper, "Stability analysis of singular patterns in the 1D Gray–Scott model: a matched asymptotics approach," *Physica D: Nonlinear Phenomena*, vol. 122, no. 1–4, pp. 1–36, 1998, doi: 10.1016/S0167-2789(98)00180-8.
- [11] M. Rodrigo and M. Mimura, "Exact solutions of reaction-diffusion systems and nonlinear wave equations," *Japan Journal of Industrial and Applied Mathematics*, vol. 18, no. 3, pp. 657–696, 2001, doi: 10.1007/BF03167410.
- [12] J.K. Hale, L.A. Peletier and W.C. Troy, "Exact homoclinic and heteroclinic solutions of the Gray–Scott model for autocatalysis," *SIAM Journal on Applied Mathematics*, vol. 61 no. 1, pp. 102–130, 2000, doi: 10.1137/S0036139998334913.
- [13] S.A. Manaa and J. Rasheed, "Successive and finite difference method for Gray–Scott model," *Science Journal of University of Zakho*, vol. 1, no. 2, pp. 862–873, 2013.
- [14] K.M. Owolabi and K.C. Patidar, "Numerical solution of singular patterns in one-dimensional Gray–Scott-like models," *International Journal of Nonlinear Sciences and Numerical Simulation*, vol. 15, no. 7–8, pp. 437–462, 2014, doi: 10.1515/ijnsns-2013-0124.
- [15] A. Korkmaz, O. Ersoy and İ. Dağ, "Motion of patterns modeled by the Gray–Scott autocatalysis system in one dimension," arXiv:1605.09712, 2016, doi: 10.48550/arXiv.1605.09712.
- [16] R.C. Mittal and R. Rohila, "Numerical simulation of reaction–diffusion systems by modified cubic B-spline differential quadrature method," *Chaos, Solitons & Fractals*, vol. 92, pp. 9–19, 2016, doi: 10.1016/j.chaos.2016.09.007.
- [17] R. Jiwari, S. Singh and A. Kumar, "Numerical simulation to capture the pattern formation of coupled reaction–diffusion models," *Chaos, Solitons & Fractals*, vol. 103, pp. 422–439, 2017, doi: 10.1016/j.chaos.2017.06.023.
- [18] A.T. Onarcan, N. Adar and İ. Dağ, "Trigonometric cubic B-spline collocation algorithm for numerical solutions of reaction–diffusion equation systems," *Computational and Applied Mathematics*, vol. 37, no. 5, pp. 6848–6869, 2018, doi: 10.1007/s40314-018-0713-4.
- [19] O.P. Yadav and R. Jiwari, "A finite element approach for analysis and computational modelling of coupled reaction–diffusion models," *Numerical Methods for Partial Differential Equations*, vol. 35, no. 2, pp. 830–850, 2019, doi: 10.1002/num.22328.
- [20] A.A.A. Amin and D.S. Mashat, "Analysis of Gray–Scott's model numerically," *American Journal of Computational Mathematics*, vol. 11, no. 4, pp. 273–288, 2021, doi: 10.4236/ajcm.2021.114018.
- [21] F. Giampaolo, M. De Rosa, P. Qi, S. Izzo and S. Cuomo, "Physics-informed neural networks approach for 1D and 2D Gray–Scott systems," *Advanced Modeling and Simulation in Engineering Sciences*, vol. 9, no. 1, p. 5, 2022, doi: 10.1186/s40323-022-00219-7.
- [22] A.T. Onarcan, N. Adar and İ. Dağ, "Numerical solutions of reaction–diffusion equation systems with trigonometric quintic B-spline collocation algorithm," *Eskişehir Technical University Journal of Science and Technology A – Applied Sciences and Engineering*, vol. 24, no. 2, pp. 121–140, 2023, doi: 10.48550/arXiv.1701.04558.
- [23] I. Ali and M.T. Saleem, "Spatiotemporal dynamics of reaction–diffusion system and its application to Turing pattern formation in a Gray–Scott model," *Mathematics*, vol. 11, no. 6, p. 1459, 2023, doi: 10.3390/math11061459.
- [24] H.K. Al-Jeaid, "A Simple Approach for Explicit Solution of the Neutron Diffusion Kinetic System," *Mathematics and Statistics*, vol. 11, no. 1, pp. 107–116, 2023, doi: 10.13189/ms.2023.110112.
- [25] L. Cappanera, G. Jaramillo and C. Ward, "Analysis and Simulation of a Nonlocal Gray–Scott Model," *SIAM Journal on Applied Mathematics*, vol. 84, no. 3, pp. 856–889, 2024, doi: 10.1137/22M1542441.
- [26] Y.A. Sabawi, S. Santra, P. Das, and N. A. Mohammad, " H^1 stability and convergence analysis of the L1/L1-2 Legendre spectral method for non-local weakly singular integro-PDEs," *Calcolo*, vol. 62, no. 4, pp. 1–46, 2025, doi: 10.1007/s10092-025-00671-y.
- [27] N. A. Mohammad, Y. A. Sabawi, and M. S. Hasso, "A compact finite-difference and Haar wavelets collocation technique for parabolic Volterra integro-differential equations," *Physica Scripta*, vol. 99, no. 12, p. 125251, 2024, doi: 10.1088/1402-4896/ad8d3d.
- [28] N. A. Mohammad, Y. A. Sabawi, and M. S. Hasso, "Numerical solution based on the Haar wavelet collocation method for partial integro-differential equations of Volterra type," *Arab Journal of Basic and Applied Sciences*, vol. 31, no. 1, pp. 614–628, 2024, doi: 10.1080/25765299.2024.2419145.
- [29] M. Asadzadeh, "An introduction to the finite element method (FEM) for differential equations," *Chalmers Lecture Notes*, 2010.
- [30] N. Kaur and V. Joshi, "Numerical solution to the Gray–Scott reaction–diffusion equation using Hyperbolic B-spline," *Journal of Physics: Conference Series*, vol. 2267, no. 1, p. 012072, 2022, doi: 10.1088/1742-6596/2267/1/012072.